RSC Advances

ROYAL SOCIETY OF CHEMISTRY

www.rsc.org/advances

RSC Advance

ARTICLE

In vitro nucleus nanoprobe with ultra-small polyethylenimine functionalized graphene quantum dots

Received 00th January 20xx,
Accepted 00th January 20xx

DOI: 10.1039/x0xx00000x

www.rsc.org/

Han Wang, Xiaomin Wang*

Graphene quantum dots surface passivated by polyethylenimine (GQDs-PEI) were prepared with a simple solvothermal method. Compared with the unfunctionalized graphene quantum dots (GQDs), the GQDs-PEI was well dispersed with an ultrasmall average diameter of ca. 1.66 nm, and has achieved a better optical property including high quantum yield (53.0%) and narrow emission spectral features which is probably because of the positively charged amines on PEI which facilitated the dispersion of GQDs. By being applied to the bioimaging of MG-63 cells, the GQDs-PEI showed brighter luminescence and minor cytotoxicity. Moreover, the GQDs-PEI is clearly rendered in the nucleus region, which offered a further application in the diagnosed of diseased phenotypes and the targeted therapy of tumour cells.

Introduction

Over the past decades, with the development of nanotechnology and biotechnology, bioimaging has experienced a rapid evolution and become a powerful tool in the diagnosis and therapy of disease since it offers a unique approach to visualize the morphological details of cells.[1, 2] Based on the fluorescent probes, bioimaging can be used for early detection of protein makers, protein diagnostics in cells and the accurate detection of nucleus which accommodates gene expression, replication, recombination and repair, as well as ribonucleic acid (RNA) processing and ribosome subunit assembly.[3-5] Organic dyes, metal ions, and traditional semiconductor quantum dots have been sequentially used as fluorescent medium but with significant drawbacks including limited water solubility, low stability, short fluorescence lifetime and easy to incur the burden of intrinsic toxicity, etc..[6, 7] Then fluorescent carbon nanoparticles have been founded and widely investigated, with the advent of large surface area, structural diversity, multifunctionality, especially low toxicity, to replace organic dyes as fluorescent probes in bioimaging.[8-11] Meanwhile, graphene, as a single-atom thick, extremely high surface area nanomaterial since first discovered in 2004, are attracting considerable attention to be a versatile platform to interact with biological molecules.[12-14] Wang et al. used large (*ca.* 100nm) graphene nanosheets loaded organic dyes as a fluorescent probe for intracellular ATP.[15] GQDs, as a new generation of carbon nanoparticles with fascinating photoluminescence properties, was first raised and reported by Dai group in 2008.[16] They found that single-layer graphene oxide sheets down to a few nanometers in lateral width, Nano-graphene oxide (NGO, as they named), exhibit intrinsic luminescence and can be used for cellular imaging with little background. In 2010, Pan et al. first introduced the concept of quantum dots and prepared Graphene Quantum Dots (GQDs) of 5-13 nm in size by cutting carboxylic reduced graphene oxide sheets through a hydrothermal approach, which exhibits bright blue photoluminescence with a quantum yield (QY) of 6.9%.[17] Then, a considerable amount of researches have been made into the preparation and surface modifying of GQDs to achieve an enhanced optical property with bright fluorescence, high photostability, large stokes shift and so on.[18-20] Jin et al. obtained ultra-small GQDs-NHR with 1-3 layers thick and less than 5 nm in diameter using a two-step cutting process with N_2H_4.[21] There also have been a few studies highlighting the application of functional GQDs in cellular imaging and most of which were well induced into cytoplasm.[22-24] However, little research of the nucleus labeling with GQDs or other fluorescent carbon nanoparticles has been conducted.

Herein, we choose polyethylenimine (PEI) to functionalize the GQDs, as it has been found to be a highly efficient vector for delivering oligonucleotides and plasmids both in vitro and in vivo, which is also one of the most efficacious membrane-disruption and non-viral agents with limit toxic effects and has been successfully used for generating core-shell fluorescent

College of Materials Science and Engineering, Taiyuan University of Technology, Taiyuan 030024, P. R. China.
Email: wangxiaomin@tyut.edu.cn; Fax: +86 351 6018639

nanoparticles (silica nanoparticles, carbon quantum dots etc.).[25-28] Ethanol was chosen as the solvent in a facile solvothermal process, which simultaneously combines the "top-down" cutting, reducing and functionalizing graphene oxide (GO) sheets in one step. It is expected that the polyethylenimine functionalized GQDs could be acquired with higher quantum efficacy, minor cytotoxicity and more easily rendered into the nucleus region, which may be further applied in bioimaging, biosensing and drug delivery system.

Results and discussion

Structural properties

GQDs-PEI was prepared by a facile one-step solvothermal reduction of GO sheets and Branched PEI (M_w = 10 000) in ethanol solution. As we know, PEI has been widely investigated with the advent of high concentration of positively charged nitrogen atoms that facilitate effective binding.[29] Herein, we propose that in the solvothermal process, the oxygen functional groups (carbonyl, carboxylic, or other) on the surface of GO sheets are passivated by the large abundant of primary, secondary and tertiary amines on BPEI (Fig. 1a-b). Therefore, the GQDs are coated with PEI to establish a Core-Shell structure, as shown in Fig. 1c. The BPEI with large amount of positively charged nitrogen atoms could promote the further cutting of GO sheets and facilitate the dispersion of GQDs, which were further proven by the TEM images.

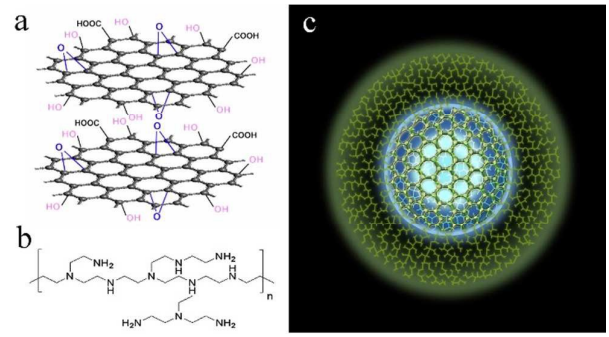

Fig. 1 (a) Simulated structure of graphene oxide sheets containing oxygen groups. (b) Structure of Branched PEI. (c) Core-Shell structure of GQDs-PEI.

Fig. 2 shows the TEM images of GQDs-PEI and GQDs, respectively. From the TEM image of the as-prepared GQDs-PEI (Fig. 2a), the collected GQDs-PEI are distributed in a narrow size between 1 and 3 nm with an average diameter of 1.66 nm, which is much smaller than its cousin (other functionalized GQDs) reported before.[30, 31] Fig. 2b shows the TEM image of the as-prepared GQDs and the inset is the average size distribution of GQDs measured by Nano Measurer. The GQDs are mostly aggregated with a bigger size between 3 and 7 nm. The results demonstrated that functionalized with PEI, the GQDs-PEI was further cut into extra small size and the aggregation was clearly ameliorated.

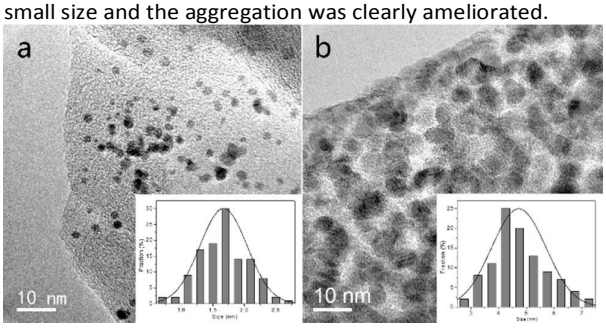

Fig. 2 (a) TEM image of the GQDs-PEI; Inset of (a): size distribution of GQDs-PEI. (b) TEM image of the GQDs; Inset of (b): size distribution of GQDs.

As shown in the Fourier transform infrared (FT-IR) spectrum (Fig. 3a), the absorption peaks of primary amine, tertiary amine and amine in different positions are clearly detected on raw PEI, among which the stretching vibration peaks between 1400cm^{-1} and 1600cm^{-1} are the characteristic peaks of PEI. After combined with GQDs (Fig. 3a, red line), the amide reaction occurred between some amine groups of PEI and the carboxyl on GO sheets, and because of the existence of the rest amine groups of PEI, the C=O peak shifts to a lower wavenumber (1672 cm^{-1}). Meanwhile, the stretching vibration peaks between 1277cm^{-1} and 1630cm^{-1} are C-N and N-H vibration peaks in amide bond. The black line in Fig. 3a is the FT-IR spectra of GO sheets， from which large amount of oxygen functional groups (carbonyl, carboxylic, or other) can be seen on the GO sheets prepared by the modified Hummers

method. It can be clearly observed that after solvothermal treatment (GQDs-PEI, red line in Fig 3a), the strong vibrational absorption band of C=O/COOH at 1630 cm^{-1} became very weak and the vibration band of epoxy groups (C=O=C) at 1045 cm^{-1} disappeared. It proves that during the solvothermal process most of the carbonyl group and epoxy groups are deoxidized.
According to the X-ray diffraction pattern (Fig. 3b), compared with GO sheets, the as-prepared GQDs-PEI were well deoxidized.

The (002) peak of GQDs-PEI is roughly 3.82 Å corresponding to a interlayer spacing of 0.382 nm, larger than that of reduced graphene Oxide (3.68).[32]

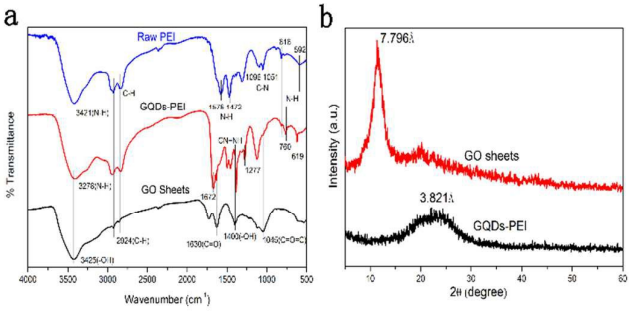

Fig. 3 (a) FTIR spectra of the raw PEI, GQDs-PEI and GO sheets. (b) XRD patterns of the GO sheets and GQDs-PEI.

Optical properties

Similar to other popular fluorescent carbon nanoparticles, the carbon nanoribbons,[33] carbon quantum dots, and other functional graphene quantum dots, both the as-synthesized GQDs-PEI and GQDs emit bright blue-green luminescence. To further explore the optical properties, a detailed PL study was carried out through different excitation wavelengths. Fig. 4a shows the normal and normalized PL emission spectra of GQDs-PEI. Similar to the GQDs reported,[17] the GQDs-PEI also exhibits an excitation-dependent PL behaviour, and the strongest excitation wavelength has a red shift from 320nm to 380 nm. When the excitation wavelength was changed from 350 to 500 nm, the PL peaks of GQDs-PEI shifted from 462 (black) to 547 nm (rose red). Fig. 4b shows the difference of UV-vis absorption and PL (at 365 nm excitation) spectra of the GQDs-PEI and GQDs without surface passivation. It is clearly revealed that the GQDs with the surface-passivation (GQDs-PEI) exhibit stronger PL and a smaller full width half maximum (FWHM). Meanwhile, the inset photographs show a brighter green fluorescence under 365 nm UV light. With the classical optical reference method,[34] the maximum quantum yield (QY) of GQDs-PEI measured and calculated by using quinine sulfate as a reference and 350 nm as the excitation wavelength is *ca.* 53.0%, much higher than GQDs without surface passivation which is 6.5% similar to the reported.[17] Another marked difference was found in the UV-vis absorption spectra of the GQDs-PEI and GQDs. Compared with GQDs, the absorption peak of GQDs-PEI is red shifted to *ca.* 340 nm with a long absorption edge.

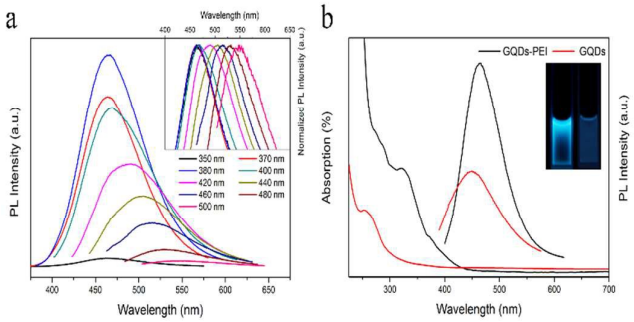

Fig. 4 (a) PL spectra for the GQDs-PEI at different excitation wavelengths（Inset: the corresponding normalized PL spectra). (b) UV-vis absorption and PLE (at 365 nm excitation) spectra of the GQDs-PEI and GQDs without functionalized (Inset: photographs of the GQDs-PEI and GQDs under 365 nm UV light).

One hypothesis for the observations is that in the solvothermal process, the presence of ethanol can deoxidize the abundant oxygen-containing functional groups that exist in the graphene oxide sheets, and on the surface of graphene oxide sheets where the epoxy groups are linearly arranged, ethanol can play an unzipping role [35], which is also confirmed by FT-IR spectra. Compared with the unfunctionalized GQDs, the existence of PEI highly improved the PL intensity of GQDs-PEI. It may because of the fact that, by adding the branched PEI, the surface of the GQDs are stabilized during the preparation phase, meanwhile, the generation of energy traps are facilitated and then light would be emitted when stimulated.[36]

Biocompatibility

Like other fluorescent nanoparticles, the GQDs are also attractive for biomedical imaging because of their stable PL, low cytotoxicity and excellent water-solubility.[37, 38] Expectation is that the biocompatibility of GQDs-PEI can also be highly improved and further applied for bioimaging, biosensing and drug delivery system. In this research, MG-63 osteoblast-like cells were used to investigate the in vitro cytotoxicity and cellular uptake of the GQDs-PEI. Different concentrations (12.5, 25, 50, 100, and 200 μg/ml) of GQDs-PEI and GQDs were incubated for 48h and cell viability was measured by MTT (3-(4, 5-dimethylthiazolyl-2) -2, 5-diphenyltetrazolium bromide) colorimetric assay, as shown in Fig. 5. The result suggested that the GQDs-PEI do not impose a considerable toxicity to MG-63 cells compared to the control (bared GQDs). It is notable that when the concentration of as-prepared GQDs-PEI was 100 μg/mL and incubation time was 48h, the cell viability was still about 80%, which indicates a minor cytotoxicity.

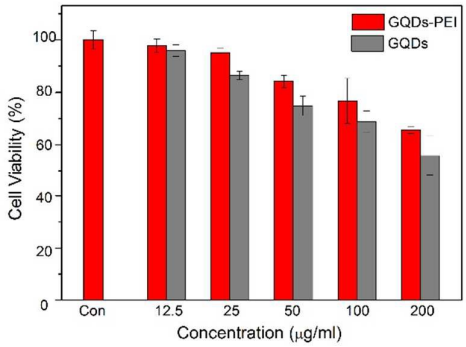

Fig. 5 Cytotoxicity evaluations test of MG-63cells with different concentrations of GQDs-PEI and GQDs after 48 h incubation

Fig. 6 shows the cellular uptake profile of GQDs-PEI and GQDs in the MG-63 cells obtained by confocal fluorescence microscopy after 6h of incubation, respectively.

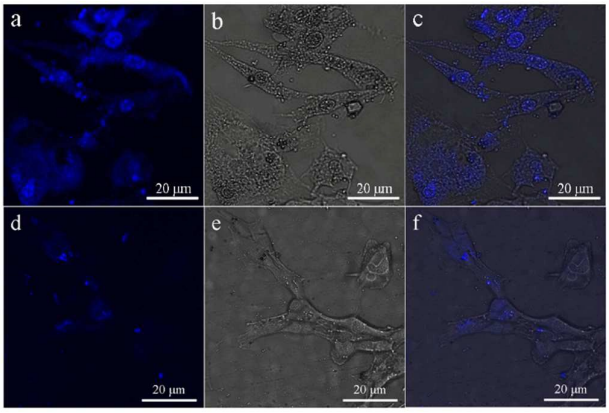

Fig. 6 (a) Confocal fluorescence microphotograph of MG-63 cells incubated with GQDs-PEI for 6h (λ_{ex} =405nm). (b) Bright-field microphotographs of cells. (c) An overlay image of (a) and (b). (d)Confocal fluorescence microphotograph of MG-63 cells incubated with GQDs for 6h (λ_{ex} =405nm). (e) Bright-field microphotographs of cells. (f) An overlay image of (d) and (e).

Fig. 6a and 6d are the confocal fluorescence microphotograph of GQDs-PEI and GQDs in MG-63 cells, from which bright blue luminescence can be clearly seen. Fig. 6b and 6e are the bright-field microphotographs of MG-63 cells incubated with GQDs-PEI and GQDs in the same region, from which we can see even after 6h incubation the MG-63 cells are still in good condition and the nucleus regions can be clearly observed. Fig. 6c and 6f are overlay images of confocal fluorescence and bright-field microphotographs. The confocal fluorescence photomicrographs corresponding to bright-field views show that both GQDs-PEI and GQDs with blue luminescence is observed inside the cells. As we expected, under the same concentration (100μg/mL) the GQDs-PEI exists a brighter luminescence. Another surprising phenomenon is that, compared with the GQDs which are mainly localized in the cytoplasm region same to other reports,[38, 39] the GQDs-PEI is clearly rendered into the nucleus region and the fluorescence is even stronger than cytoplasm, as shown in Fig. 6c.

To further confirm that the as-prepared GQDs-PEI can render into cell nucleus, a nucleus co-localization experiment was carried out with the commonly used nucleus dye, 4', 6-diamidino-2-phenylindole (DAPI). To double-check the nucleus permeability of GQDs-PEI, another set of mouse osteoblastic cells MC3T3-E1 is used in this experiment.

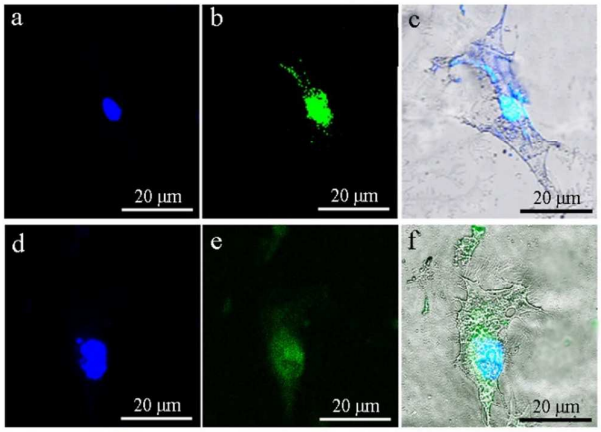

Fig. 7 (a) and (d) Confocal fluorescence microphotograph of DAPI distributed in MC3T3-E1 cells (λ ex =405nm); (b) and (e) Confocal fluorescence microphotograph of GQDs-PEI distributed in MC3T3-E1 cells (λ ex =488nm); (c), and (f) Overlay image of confocal fluorescence and bright-field microphotographs, respectively.

Fig. 7a and 7d show the confocal fluorescence microphotographs of DAPI distributed in MC3T3-E1 cells (λ_{ex} =405nm). The bright blue nucleus regions are dyed with DAPI and thus can be easily localized. Fig. 7b and 7e show the distribution of GQDs-PEI in the same regions (λ_{ex} =488nm). Bright green luminescence of GQDs-PEI was clearly observed and is distributed over a larger area. Fig. 7c and 7f are overlay images of confocal fluorescence and bright-field microphotographs, respectively. The confocal fluorescence photomicrographs corresponding to bright-field views show that GQDs-PEI with green luminescence is observed inside the cells. Furthermore, in the nucleus region where DAPI accumulated, GQDs-PEI with green luminescence is also observed, which finally confirms the nucleus permeability of GQDs-PEI. It is also noticed that the luminescence of GQDs-PEI at nucleus region is much stronger than in cytoplasm. This is probably because the nucleus regions of more genetic material always have a greater density than the cytoplasm, and the weak acid environment making it more conducive to the aggregation of alkaline nanoparticles.[5]
This nucleus permeability of GQDs-PEI may attribute to the ultra-small size of GQDs-PEI and high concentration of positively charged nitrogen atoms of PEI， which also means an excellent membrane-disruption ability. The results suggest that GQDs-PEI could be considered as a promising agent for gene probes and drug delivery systems. Further studies should be provided for in vitro and in vivo applications, and for actual applications in the human body.

Experimental

Reagents

Branched Polyethylenimine (BPEI, average molecular weight: 10kDa) and quinine sulfate fluorescence standard substance were purchased from Aladdin Industrial Inc., Shanghai (China). MG-63 osteoblast-like cells and mouse osteoblastic cells MC3T3-E1 were purchased from Cell Bank of the Chinese Academy of Sciences, Shanghai (China). MTT and DAPI were purchased from Beyotime Institute of Biotechnology, Jiangsu (China). Ultrapure water (18 MΩ·cm^{-1}) was used in entire experimental procedures.

Preparation of GQDs surface-passivated by PEI

Graphene oxide (GO) sheets were prepared from graphite powder by a modified Hummers method.[40] The GO sheets (50 mg) were dispersed in 40ml ethanol. PEI 10000 (200mg) was added into the solution under thoroughly stirred, and then the PH was turned to 12 with ammonia solution (28 wt% in water). Then, the mixture solution was transferred into a 100 mL Teflon-lined stainless-steel autoclave and heated at 200 ℃ for 20 hours. After cooling to room temperature, the resulting suspension was filtered through a 0.22 μm microporous membrane, and the colloidal solution were further purified and separated via column chromatography on neutral Aluminium oxide to remove the excess PEI. With ethanol as the eluent, GQDs-PEI with blue fluorescence was obtained.
The GQDs without surface-passivation were also prepared for the comparison (the same preparation process with GQDs-PEI, only without PEI).

In Vitro Cytotoxicity and Fluorescence Imaging

To investigate the in vitro toxicity of GQDs-PEI, GQDs-PEI and GQDs have been loaded with MG-63 cells over 48 hours. Specifically, in a 96-well plate, 100 μL suspension of MG-63 cells (4×10^{4}cells/mL) in Minimum Essential Medium (MEM, GIBCO, containing $NaHCO_3$ 1.5g/L and Sodium Pyruvate 0.11g/L) supplemented with 10% fetal bovine serum were added to each well and incubated in a 5% CO_2 humidified incubator at 37 °C for 24 hours. Then, the GQDs-PEI and GQDs with a concentration of

12.5, 25, 50, 100 and 200 μg/mL were added into those wells respectively, each concentration of samples occupying five wells and being incubated for additional 48 hours. The medium was then removed and cells were washed with phosphate-buffered saline. After 100 μL of MTT solution with a concentration of 0.5 mg/mL in culture medium was prepared and added to each well, the 96-well plate being further incubated for another 4 hours, after the culture medium with MTT being removed and 100 μL of DMSO was added, the resulting mixtures was kept shaken for 10 min at room temperature. Finally, the optical density of the mixtures was measured at a wavelength of 490 nm and then the cell viability was expressed as percentage of absorbance relative to control which was obtained in the absence of the samples (GQDs-PEI and GQDs).

For a fluorescent cellular imaging of GQDs-PEI and GQDs, 1 mL suspension of MG-63 cells (4×10^4cells/mL) were seeded in each well of a 12-well plate and cultured at 37 °C for 24 hours. The aqueous solution of GQDs-PEI and GQDs (2 mg/mL) went through a 0.2 μm sterile filter membrane, separately. The filtered fluorescent suspension (50 μL) was mixed with the culture medium (950 μL) and then added to each well (three wells per sample and the fourth was used as a control) in which the MG-63 cells were grown. After an incubation of 6 h, the medium was removed and the cells were washed thoroughly three times with PBS (500 μL each time) to remove the free particles from the cells. A confocal microscopy was used to observe the cellular uptake situation for both GQDs-PEI and GQDs by MG-63 cells under 405 nm excitation. The nucleus co-localization experiment was conducted follow the same procedure with mouse osteoblastic cells MC3T3-E1.

Instruments

JEOL JEM 2010 microscope (JEOL, Japan) with acceleration voltage of 200 kV was used for the High-resolution TEM images. The FT-IR spectrum was obtained with a Bruker Tensor 27 Fourier transform infrared spectrometer (Germany) and the XRD spectrum was recorded by TD-3500 Automatic X-ray diffractometer System (Dandong, China). The UV-vis and Photoluminescence (PL) spectra of the samples dispersed in ethanol were collected by using a Horiba Jobin Yvon Fluromax-4 spectrofluorometer (Japan) and Hitachi U-3900 UV-vis spectrophotometer, respectively, and recorded with quartz cells of 10 mm path length. The absorbance of the MTT colorimetric assay was quantified spectrophotometrically by a Tecan Infinite F50 microplate reader (Tecan Group, Mannedorf, Switzerland). The confocal fluorescence microscope was examined by a Nikon C2 Plus confocal laser scanning microscope (Nikon Corp, Japan).

Conclusions

This study demonstrates the nucleus labeling property of graphene quantum dots surface passivated with branched PEI. Ultra-small GQDs-PEI were synthesized with a new convenient solvothermal method which combined the “top-down” cutting, reducing and functionalizing graphene oxide (GO) sheets in one step. The morphology and structure of GQDs-PEI were investigated by TEM, FT-IR and XRD spectroscopic analysis. Compared with the unfunctionalized GQDs, the GQDs-PEI has achieved a better optical property including high quantum yield (maximum value is 53.0%) and narrow emission spectral features. The MTT assays of cell viability studies further suggested that the GQDs-PEI do not impose a considerable toxicity of MG-63 cells compared to the GQDs. Moreover, different with the GQDs family members which are mainly localized in the cytoplasm region, cell images observed by confocal microscope have demonstrated that the GQDs-PEI are mainly aggregated in the nucleus region which may find exciting applications in the nucleus labeling, diseased phenotypes diagnosing and the targeted therapy of tumour cells.

Acknowledgements

This work is supported by the National Natural Science Foundation of China (51372160 and 51172152).

Notes and references

1. M. Chen and M. Yin, *Progress in Polymer Science*, 2014, **39**, 365-395.
2. D.-E. Lee, H. Koo, I.-C. Sun, J. H. Ryu, K. Kim and I. C. Kwon, *Chemical Society Reviews*, 2012, **41**, 2656.
3. K. Y. Pu, K. Li, X. Zhang and B. Liu, *Adv Mater*, 2010, **22**, 4186-4189.
4. N. L. Rosi and C. A. Mirkin, *Chemical Reviews*, 2005, **105**, 1547-1562.
5. Y. Ding, Q. Wu, K. Zheng, L. An, X. Hu and W. Mei, *RSC Advances*, 2015, **5**, 63330-63337.
6. U. Resch-Genger, M. Grabolle, S. Cavaliere-Jaricot, R. Nitschke and T. Nann, *Nature methods*, 2008, **5**, 763-775.
7. X. Liu, Y. Gao, X. Wang, S. Wu and Z. Tang, *Journal of Nanoscience and Nanotechnology*, 2011, **11**, 1941-1949.
8. Y.-P. Sun, B. Zhou, Y. Lin, W. Wang, K. S. Fernando, P. Pathak, M. J. Meziani, B. A. Harruff, X. Wang and H. Wang, *Journal of the American Chemical Society*, 2006, **128**, 7756-7757.
9. Z. Tao, G. Hong, C. Shinji, C. Chen, S. Diao, A. L. Antaris, B. Zhang, Y. Zou and H. Dai, *Angewandte Chemie*, 2013, **125**, 13240-13244.
10. S. Diao, G. Hong, J. T. Robinson, L. Jiao, A. L. Antaris, J. Z. Wu, C. L. Choi and H. Dai, *Journal of the American Chemical Society*,

2012, **134**, 16971-16974.
11. Y. Zhao, Q. Liu, S. Shakoor, J. R. Gong and D. Wang, *Toxicology Research*, 2015, **4**, 270-280.
12. K. S. Novoselov, A. K. Geim, S. Morozov, D. Jiang, Y. Zhang, S. Dubonos, I. Grigorieva and A. Firsov, *science*, 2004, **306**, 666-669.
13. V. C. Sanchez, A. Jachak, R. H. Hurt and A. B. Kane, *Chemical Research in Toxicology*, 2012, **25**, 15-34.
14. X. Yang, J. Zhu, L. Qiu and D. Li, *Advanced materials*, 2011, **23**, 2833-2838.
15. Y. Wang, Z. Li, D. Hu, C.-T. Lin, J. Li and Y. Lin, *Journal of the American Chemical Society*, 2010, **132**, 9274-9276.
16. X. Sun, Z. Liu, K. Welsher, J. T. Robinson, A. Goodwin, S. Zaric and H. Dai, *Nano Research*, 2008, **1**, 203-212.
17. D. Pan, J. Zhang, Z. Li and M. Wu, *Advanced Materials*, 2010, **22**, 734-738.
18. M. Zhang, L. Bai, W. Shang, W. Xie, H. Ma, Y. Fu, D. Fang, H. Sun, L. Fan, M. Han, C. Liu and S. Yang, *Journal of Materials Chemistry*, 2012, **22**, 7461.
19. V. Gupta, N. Chaudhary, R. Srivastava, G. D. Sharma, R. Bhardwaj and S. Chand, *Journal of the American Chemical Society*, 2011, **133**, 9960-9963.
20. S. H. Song, M. H. Jang, J. Chung, S. H. Jin, B. H. Kim, S. H. Hur, S. Yoo, Y. H. Cho and S. Jeon, *Advanced Optical Materials*, 2014, **2**, 1016-1023.
21. S. H. Jin, D. H. Kim, G. H. Jun, S. H. Hong and S. Jeon, *Acs Nano*, 2013, **7**, 1239-1245.
22. C. Hu, Y. Liu, Y. Yang, J. Cui, Z. Huang, Y. Wang, L. Yang, H. Wang, Y. Xiao and J. Rong, *Journal of Materials Chemistry B*, 2013, **1**, 39.
23. M. Nurunnabi, Z. Khatun, M. Nafiujjaman, D. G. Lee and Y. K. Lee, *ACS Appl Mater Interfaces*, 2013, **5**, 8246-8253.
24. Q. Xue, H. Huang, L. Wang, Z. Chen, M. Wu, Z. Li and D. Pan, *Nanoscale*, 2013, **5**, 12098-12103.
25. S. N. Baker and G. A. Baker, *Angewandte Chemie International Edition*, 2010, **49**, 6726-6744.
26. O. Boussif, F. Lezouale'H, M. A. zanta, M. D. Mergny, D. Scherman, B. Demeneix and J.-P. Behr, *Proceedings of the National Academy of Sciences of the United States of Amercia*, 1995, **92**, 7297-7301.
27. C. Liu, P. Zhang, X. Zhai, F. Tian, W. Li, J. Yang, Y. Liu, H. Wang, W. Wang and W. Liu, *Biomaterials*, 2012, **33**, 3604-3613.
28. J. E. Fuller, G. T. Zugates, L. S. Ferreira, H. S. Ow, N. N. Nguyen, U. B. Wiesner and R. S. Langer, *Biomaterials*, 2008, **29**, 1526-1532.
29. Z. Dai, T. Gjetting, M. A. Mattebjerg, C. Wu and T. L. Andresen, *Biomaterials*, 2011, **32**, 8626-8634.
30. X. Yan, X. Cui and L.-s. Li, *Journal of the American Chemical Society*, 2010, **132**, 5944-5945.
31. J. Lu, P. S. E. Yeo, C. K. Gan, P. Wu and K. P. Loh, *Nature nanotechnology*, 2011, **6**, 247-252.
32. J. Shen, Y. Zhu, X. Yang, J. Zong, J. Zhang and C. Li, *New Journal of Chemistry*, 2012, **36**, 97.
33. J. Lu, J.-x. Yang, J. Wang, A. Lim, S. Wang and K. P. Loh, *ACS nano*, 2009, **3**, 2367-2375.
34. J. N. Demas and G. A. Crosby, *The Journal of Physical Chemistry*, 1971, **75**, 34.
35. D. V. Kosynkin, A. L. Higginbotham, A. Sinitskii, J. R. Lomeda, A. Dimiev, B. K. Price and J. M. Tour, *Nature*, 2009, **458**, 872-876.
36. B. Han, W. Wang, H. Wu, F. Fang, N. Wang, X. Zhang and S. Xu, *Colloids and Surfaces B: Biointerfaces*, 2012, **100**, 209-214.
37. H. Sun, L. Wu, N. Gao, J. Ren and X. Qu, *ACS applied materials & interfaces*, 2013, **5**, 1174-1179.
38. Q. Liu, B. Guo, Z. Rao, B. Zhang and J. R. Gong, *Nano letters*, 2013, **13**, 2436-2441.
39. J. Peng, W. Gao, B. K. Gupta, Z. Liu, R. Romero-Aburto, L. Ge, L. Song, L. B. Alemany, X. Zhan and G. Gao, *Nano letters*, 2012, **12**, 844-849.
40. D. Li, M. B. Muller, S. Gilje, R. B. Kaner and G. G. Wallace, *Nat Nanotechnol*, 2008, **3**, 101-105.

RSC Advance

ARTICLE